Electro–magnetic control of shear flow over a cylinder for drag reduction and lift enhancement*

Zhang Hui(张 辉)†, Fan Bao-Chun(范宝春), Chen Zhi-Hua(陈志华), Chen Shuai(陈 帅), and Li Hong-Zhi(李鸿志)

Science and Technology on Transient Physics Laboratory, Nanjing University of Science and Technology, Nanjing 210094, *China*

(Received 6 December 2012; revised manuscript received 5 March 2013)

In this paper, the electro–magnetic control of a cylinder wake in shear flow is investigated numerically. The effects of the shear rate and Lorentz force on the cylinder wake, the distribution of hydrodynamic force, and the drag/lift phase diagram are discussed in detail. It is revealed that Lorentz force can be classified into the field Lorentz force and the wall Lorentz force and they affect the drag and lift forces independently. The drag/lift phase diagram with a shape of "8" consists of two closed curves, which correspond to the halves of the shedding cycle dominated by the upper and lower vortices respectively. The free stream shear ($K > 0$) induces the diagram to move downward and leftward, so that the average lift force directs toward the downside. With the upper Lorentz force, the diagram moves downwards and to the right by the field Lorentz force, thus resulting in the drag increase and the lift reduction, whereas it moves upward and to the left by the wall Lorentz force, leading to the drag reduction and the lift increase. Finally the diagram is dominated by the wall Lorentz force, thus moving upward and leftward. Therefore the upper Lorentz force, which enhances the lift force, can be used to overcome the lift loss due to the free stream shear, which is also obtained in the experiment.

Keywords: cylinder wake control, Lorentz force, shear flow, hydrodynamic force

PACS: 47.15.Cb, 47.85.L– **DOI:** 10.1088/1674-1056/22/10/104701

1. Introduction

Ever since the period of vortex shedding of a bluff body was measured by Roshko (1955),[1] vortex shedding has been attracting much attention in the field of fluid dynamics.[2–8] There exist plenty of results from theoretical, experimental, and numerical approaches for the flow through a circular cylinder.

Most of the bluff-body flows with an engineering background are shear flows. The simplest case is a uniform-shear flow past through an isolated circular cylinder, with a linear distribution of the velocity components in the lateral direction and an infinite lateral width of the flow domain. Part of the early studies on shear flow were summarized by Jordon and Fromm, which mainly focused on the shift of the front stagnation point[9,10] and the motion of the separation points.[11] Recently, Lei *et al*. (2000)[12] and Kang (2006)[13] have paid more attention to the effects of Reynolds number and shear rate on the vortex-shedding frequency. Meanwhile, experimental studies on shear flow have also been reported by Kiya *et al*. (1980),[14] Kwon *et al*. (1992),[15] Hayashi *et al*. (1993),[6] and Sumner and Akosile(2003).[17] However, it is clear that there still remain some uncertainties regarding the vortex shedding and hydrodynamic forces acting on a circular cylinder in shear flow, and more investigations on the uniform-shear flow are necessary.

In addition, as a bluff-body is immersed in shear flow, a negative lift force may be generated, similar to the stall phenomenon encountered in airfoils at high attack angles, which is generally undesirable from a practical point of view. Therefore, investigations on the control of shear flow over a cylinder are also necessary due to the practical and theoretical importance. Electro–magnetic control is considered as one of the most practical methods developed so far, in which the Lorentz force generated by an electro–magnetic actuator in an electrically conducting fluid (such as sea water) is used to manipulate the flow.[18–22] Regarding the flow through a circular cylinder, Crawford and Karniadakis,[23] Weier *et al*.,[24] Kim and Lee,[25] and Posdziech and Grundmann[26] investigated the effects of Lorentz force on the elimination of flow separation and drag reduction by both experiments and calculations. The control of cylinder wake with Lorentz forces was also performed experimentally and numerically by our research group.[27–30]

In this paper, the electro–magnetic control of a cylinder wake in shear flow is investigated numerically. The numerical investigation is conducted by using the alternative–direction implicit (ADI) algorithm and the fast Fourier transform (FFT) algorithm based on the governing equations in the exponential–polar coordinates. The distributions of hydrodynamic forces on the cylinder surface, i.e., wall pressure, drag, and lift induced by the Lorentz force are directly obtained from the corresponding equations derived in the paper. It is suggested that the Lorentz force can be classified into the field

*Project supported by the National Natural Science Foundation of China (Grant Nos. 11202102 and 11172140) and the Specialized Research Fund for Doctoral Program of High Education, China (Grant No. 20123219120050).

†Corresponding author. E-mail: zhanghui1902@hotmail.com

© 2013 Chinese Physical Society and IOP Publishing Ltd

Lorentz force and the wall Lorentz force[29] and the velocity field is only affected by the field Lorentz force.

Based on the numerical results, it is confirmed that the shear flow over a cylinder can be controlled to keep the lift positive by the electro–magnetic actuator applied only to the half surface of the cylinder. In order to deepen the understanding of the control mechanism further, the drag–lift phase diagram is employed, which not only denotes the corresponding fluctuation of the drag and lift over a complete time period, but also implies detailed information about the flow patterns in the wake and the time history of the fluctuating pressures on the cylinder surface. The effects of the shear rate, the field, and wall Lorentz forces on the drag–lift phase diagram are also discussed in detail in the paper.

2. Governing equations

Considering an incompressible electrically conducting viscous flow with an applied Lorentz force generated by electro–magnetic actuator covered on a circular cylinder immerged in fluid vertically, the governing equations in the exponential–polar coordinates (ξ,η), $r=\mathrm{e}^{2\pi\xi}$, and $\theta=2\pi\eta$, can be written in the dimensionless form as

$$\begin{aligned} &H\frac{\partial\Omega}{\partial t}+\frac{\partial(U_r\Omega)}{\partial\xi}+\frac{\partial(U_\theta\Omega)}{\partial\eta}\\ &=\frac{2}{Re}\left(\frac{\partial^2\Omega}{\partial\xi^2}+\frac{\partial^2\Omega}{\partial\eta^2}\right)\\ &\quad+NH^{1/2}\left(\frac{\partial F_\theta}{\partial\xi}+2\pi F_\theta-\frac{\partial F_r}{\partial\eta}\right), \qquad (1)\\ &\frac{\partial^2\psi}{\partial\xi^2}+\frac{\partial^2\psi}{\partial\eta^2}=-H\Omega, \qquad (2)\end{aligned}$$

where the stream function ψ is defined as $\partial\psi/\partial\eta=U_r=H^{1/2}u_r$, $-\partial\psi/\partial\xi=U_\theta=H^{1/2}u_\theta$; vorticity Ω is defined as

$$\Omega=\frac{1}{H}\left(\frac{\partial U_\theta}{\partial\xi}-\frac{\partial U_r}{\partial\eta}\right),$$

with u_r and u_θ being the velocity components in r an θ directions, respectively; $H=4\pi^2\mathrm{e}^{4\pi\xi}$; $Re=2u_\infty a/\nu$, with u_∞ being the free-stream velocity (at $\theta=0$), ν the kinematic viscosity, and a the cylinder radius; the non-dimensional time is $t=t^*u_\infty/a$; the interaction parameter is defined as $N=j_0B_0a/\rho u_\infty^2$, with the current density $j_0=\sigma E_0$, σ the electric conductivity, E_0 the electric field, and B_0 the magnetic field.

The Lorentz force $\boldsymbol{F}$ is defined as[24,26]

$$\begin{aligned} F_r &= 0,\\ F_\theta &= \mathrm{e}^{-\alpha(r-1)}g(\theta) \quad \text{with} \quad g(\theta)\\ &= \begin{cases} 1, & \text{covered with actuator on upper surface,}\\ -1, & \text{covered with actuator on lower surface,}\\ 0 & \text{elsewhere,}\end{cases}\end{aligned}$$

where the value α describes the electromagnetic penetration into the fluid.

A uniform plane shear flow with a linear velocity profile $U=U_\infty+Gy$[12] is taken as the inflow in the paper as shown in Fig. 1, where y is the coordinate in the lateral direction, U_∞ and G are the central streamwise velocity (at $\theta=0$) and the lateral velocity gradient, respectively, then the initial flow field is obtained through the analytic solutions of a non-viscous flow. At $t=0$,

$$\begin{aligned}\psi &= -2\,\mathrm{sh}\,(2\pi\xi)\sin(2\pi\eta)\\ &\quad-\frac{K}{2}\left[\mathrm{sh}\,(4\pi\xi)\cos(4\pi\eta)-\mathrm{e}^{2\pi\xi}\,\mathrm{sh}\,(2\pi\xi)\right],\ \ \Omega=K. \qquad (3)\end{aligned}$$

At $t>0$, on the cylinder surface $\xi=0$, where the no-slip boundary condition is used

$$\psi=0,\quad \Omega=-\frac{1}{H}\frac{\partial^2\psi}{\partial\xi^2}. \qquad (4)$$

Away from the cylinder, $\xi=\xi_\infty$

$$\begin{aligned}\psi &= -2\,\mathrm{sh}\,(2\pi\xi)\sin(2\pi\eta)\\ &\quad-\frac{K}{2}\left[\mathrm{sh}\,(4\pi\xi)\cos(4\pi\eta)-\mathrm{e}^{2\pi\xi}\,\mathrm{sh}\,(2\pi\xi)\right],\ \ \Omega=K, \qquad (5)\end{aligned}$$

where $K=2Ga/U_\infty$ is shear rate characterizing the shear flow over a cylinder.

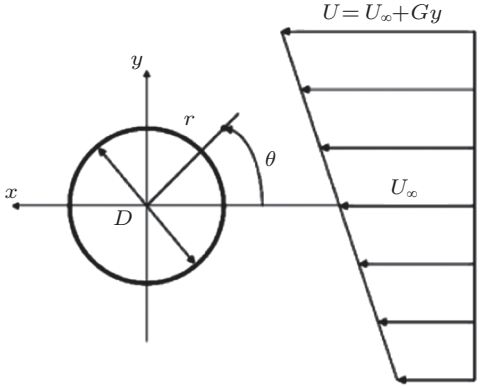


Fig. 1. Definition sketch of shear flow over circular cylinder.

It is obvious[29] that the Lorentz force on the wall, denoted by $F_\theta|_{\xi=0}$, does not have any effect on the stream function/vorticity fields due to the non-slip boundary, and the velocity field is also independent of $F_\theta|_{\xi=0}$ sequentially. Namely, the stream function/vorticity and velocity fields are only affected by the field Lorentz force $F_\theta|_{\xi>0}$.

3. Hydrodynamic force

A net hydrodynamic force $\mathbb{F}^\theta$ will be exerted on a circular cylinder as it is immersed in a fluid, which can be defined in the dimensionless form as

$$C_F^\theta=\frac{\mathbb{F}^\theta}{\frac{1}{2}\rho u_\infty^2}=\sqrt{\left(\frac{\mathbb{F}_\tau^\theta}{\frac{1}{2}\rho u_\infty^2}\right)^2+\left(\frac{\mathbb{F}_p^\theta}{\frac{1}{2}\rho u_\infty^2}\right)^2}$$

$$= \sqrt{(C_\tau^\theta)^2 + (C_p^\theta)^2}, \tag{6}$$

where shear stress C_τ^θ generated due to the velocity gradient on the boundary is expressed as

$$C_\tau^\theta = \frac{4}{Re}\Omega, \tag{7}$$

and pressure coefficient C_p^θ is defined as

$$C_p^\theta = P_\theta - P_\infty, \tag{8}$$

where the dimensionless pressure is $P = p/(\rho u_\infty^2/2)$ with p being the pressure of the flow field. Then, C_p^θ can be formulated further by the following mathematical derivation.

The momentum equations with the source of Lorentz force are

$$\begin{aligned}\frac{\partial P}{\partial \xi} &= -4\pi e^{2\pi\xi}\frac{\partial u_r}{\partial t} - 2u_r\frac{\partial u_r}{\partial \xi} - 2u_\theta\frac{\partial u_r}{\partial \eta} \\ &\quad + 4\pi u_\theta^2 - \frac{4}{Re}\frac{\partial \Omega}{\partial \eta}, \end{aligned}\tag{9}$$

$$\begin{aligned}\frac{\partial P}{\partial \eta} &= -4\pi e^{2\pi\xi}\frac{\partial u_\theta}{\partial t} - 2u_r\frac{\partial u_\theta}{\partial \xi} - 2u_\theta\frac{\partial u_\theta}{\partial \eta} \\ &\quad + 4\pi u_r u_\theta + \frac{4}{Re}\frac{\partial \Omega}{\partial \xi} + 4\pi N F_\theta. \end{aligned}\tag{10}$$

On the surface of the cylinder $\boldsymbol{u} = 0$, equation (10) becomes

$$\left[\frac{\partial P}{\partial \eta} = \frac{4}{Re}\frac{\partial \Omega}{\partial \xi} + 4\pi N F_\theta\right]_{\xi=0}. \tag{11}$$

Integrating Eq. (11) in the η direction from $\eta = 0$ to η, one obtains

$$P_\theta - P_0 = \frac{4}{Re}\int_0^\eta \frac{\partial \Omega}{\partial \xi}\,d\eta + 4\pi N\int_0^\eta F_\theta|_{\xi=0}\,d\eta. \tag{12}$$

Integrating Eq. (9) in the ξ direction from $\xi = 0$ to ξ, one obtains

$$\begin{aligned}P_\infty - P_0 &= -4\pi\int_0^\infty \frac{\partial u_r}{\partial t} e^{2\pi\xi}\,d\xi - 1 - 2\int_0^\infty u_\theta\frac{\partial u_r}{\partial \eta}\,d\xi \\ &\quad + 4\pi\int_0^\infty u_\theta^2\,d\xi - \frac{4}{Re}\int_0^\infty \frac{\partial \Omega}{\partial \eta}\,d\xi. \end{aligned}\tag{13}$$

Then

$$C_p^\theta = P_\theta - P_\infty = C_{p\mathrm{F}}^\theta + C_{p\mathrm{W}}^\theta, \tag{14}$$

where

$$C_{p\mathrm{F}}^\theta = \frac{4}{Re}\int_0^\eta \frac{\partial \Omega}{\partial \xi}\,d\eta + C_p^0, \tag{15}$$

$$\begin{aligned}C_p^0 &= 1 + 4\pi\int_0^\infty \frac{\partial u_r}{\partial t} e^{2\pi\xi}\,d\xi + 2\int_0^\infty u_\theta\frac{\partial u_r}{\partial \eta}\,d\xi \\ &\quad - 4\pi\int_0^\infty u_\theta^2\,d\xi + \frac{4}{Re}\int_0^\infty \frac{\partial \Omega}{\partial \eta}\,d\xi, \end{aligned}\tag{16}$$

$$C_{p\mathrm{W}}^\theta = 4\pi N\int_0^\eta F_\theta|_{\xi=0}\,d\eta. \tag{17}$$

Subscript 'F' represents the wall pressure induced by the field Lorentz force $F_\theta|_{\xi>0}$ and 'W' denotes the wall pressure induced by the wall Lorentz force $F_\theta|_{\xi=0}$.

The hydrodynamic force is also regarded as a force consisting of drag force and lift force denoting the force components in the streamwise and the normal directions, respectively. Then, the distribution of drag force, which consists of pressure drag $C_p^\theta\cos\theta$ and friction drag $C_\tau^\theta\sin\theta$, can be expressed as

$$C_d^\theta = C_p^\theta\cos\theta + C_\tau^\theta\sin\theta = C_{d\mathrm{F}}^\theta + C_{d\mathrm{W}}^\theta, \tag{18}$$

where

$$C_{d\mathrm{F}}^\theta = C_{p\mathrm{F}}^\theta\cos\theta + C_\tau^\theta\sin\theta, \tag{19}$$

$$C_{d\mathrm{W}}^\theta = C_{p\mathrm{W}}^\theta\cos\theta = 4\pi N\cos\theta\int_0^\eta F_\theta|_{\xi=0}\,d\eta. \tag{20}$$

Subscripts 'F' and 'W' represent the field Lorentz force and the wall Lorentz force respectively.

Similarly, the distribution of lift force can be expressed as

$$C_l^\theta = C_p^\theta\sin\theta + C_\tau^\theta\cos\theta = C_{l\mathrm{F}}^\theta + C_{l\mathrm{W}}^\theta, \tag{21}$$

$$C_{l\mathrm{F}}^\theta = C_{p\mathrm{F}}^\theta\sin\theta + C_\tau^\theta\cos\theta, \tag{22}$$

$$C_{l\mathrm{W}}^\theta = C_{p\mathrm{W}}^\theta\sin\theta = 4\pi N\sin\theta\int_0^\eta F_\theta|_{\xi=0}\,d\eta. \tag{23}$$

The total force is obtained by integrating the force distribution function along the cylinder surface. By defining the dimensionless form

$$C = \frac{F}{\rho u_\infty^2 a},$$

we can then write

$$C_d = \int_0^{2\pi} C_d^\theta\,d\theta = C_{d\mathrm{F}} + C_{d\mathrm{W}} \tag{24}$$

and

$$C_l = \int_0^{2\pi} C_l^\theta\,d\theta = C_{l\mathrm{F}} + C_{l\mathrm{W}}, \tag{25}$$

where

$$C_{d\mathrm{F}} = \frac{2}{Re}\int_0^1 \left(2\pi\Omega - \frac{\partial \Omega}{\partial \xi}\right)\sin(2\pi\eta)\,d\eta, \tag{26}$$

$$C_{d\mathrm{W}} = -2\pi N\int_0^1 F_\theta|_{\xi=0}\sin(2\pi\eta)\,d\eta, \tag{27}$$

$$C_{l\mathrm{F}} = \frac{2}{Re}\int_0^1 \left(2\pi\Omega - \frac{\partial \Omega}{\partial \xi}\right)\cos(2\pi\eta)\,d\eta, \tag{28}$$

$$C_{l\mathrm{W}} = -2\pi N\int_0^1 F_\theta|_{\xi=0}\cos(2\pi\eta)\,d\eta. \tag{29}$$

The calculations have been performed numerically at $Re = 150$ with the computational step size $\Delta\xi = 0.004$, $\Delta\eta = 0.002$, and $\Delta t = 0.005$. The equation of vorticity transport is solved by using the alternative-direction implicit (ADI) algorithm, and the equation of stream function is integrated by means of a fast Fourier transform (FFT) algorithm. More details can be found in Refs. [18], [28]–[30].

4. Numerical results and discussion

A sequence of numerical results of cylinder wake for a shear flow with $Re = 150$ and $K = 0.46$ at four special time instants of a shedding cycle is exhibited by the shaded vorticity contours in Fig. 2. It is noteworthy that the asymmetry of the free stream causes a shift of the front stagnation point towards the high velocity side, and results in the decline of vortex streets towards the lower velocity side. The mirrored symmetry in the case of $K = 0$ (uniform flow) is broken.

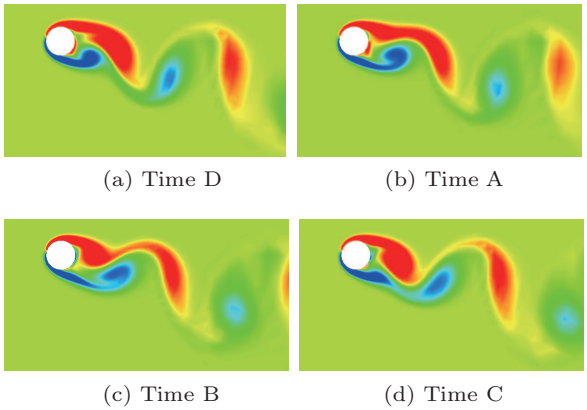


Fig. 2. (color online) Calculated vorticity contours of cylinder wake with shear rate $K = 0.46$.

The variation of flow field leads to the variation of drag and lift. One periodic behavior of the lift and drag forces can be represented more clearly in the form of phase diagram by plotting Cd as a function of Cl, which has a closed shape corresponding to a Lissajou figure of "8" as shown in Fig. 3 where the letters A, B, C, and D correspond to Time A, Time B, Time C, and Time D, respectively, in Fig. 2. For $K = 0$, the phase diagram is symmetric about the line of $Cl = 0$. For $K > 0$, the flow symmetry is broken, which leads to the asymmetry of the phase diagram. The average lift force becomes negative (directed toward the downside) and decreases with the increase of shear rate K due to the shift of the front stagnation point. In addition, the across point (A and C) in the phase diagram moves downward and leftward with the increase of shear rate K.

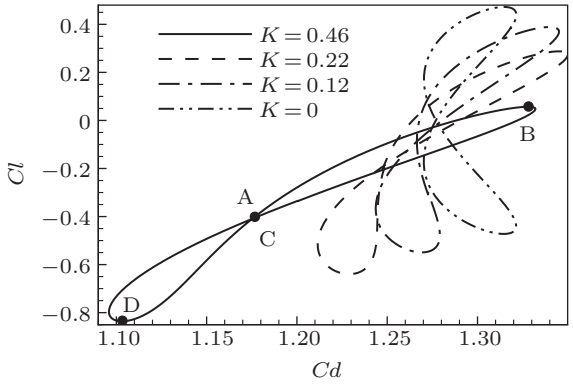


Fig. 3. Variations of drag–lift phase diagram with shear rate K.

As mentioned above, the average lift force will become negative for the cylinder immersed in a shear flow with shear rate $K > 0$, which is similar to the stall phenomenon encountered in the case of airfoils at high attack angles. In order to enhance the lift in a shear flow, the cylinder wake controlled by upper Lorentz force is discussed here.

Figure 4 shows the numerical visualizations by vorticity contours under the action of upper Lorentz force in a shear flow with $N = 0.5$ and $K = 0.46$, which leads to the increase of the vorticity, and the elongation of the shear layer connected with the upper surface of the cylinder. Moreover, it is obvious that the basic characteristics of the shear flow remain after the action of Lorentz force, such as the shift of stagnation point to the fast side of the free-steam, the incline of vortex street toward the slow side of the free-stream, etc.

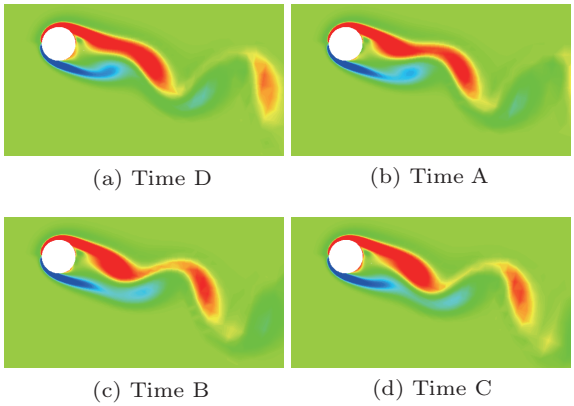


Fig. 4. (color online) Calculated vorticity contours of the cylinder wake in shear flow with the action of upper Lorentz force ($N = 0.5$ and $K = 0.46$).

Since the pressure is one order of magnitude larger than the shear stress,[31,32] it is essential to know exactly the pressure distribution on the cylinder surface to further understand the effect of the flow over the cylinder on the hydrodynamic force.

The hydrodynamic force induced by field Lorentz force is dependent on flow field. The distributions of $C_{p\mathrm{F}}^{\theta}$ at a given instant A are shown in Fig. 5, where the dashed line represents the shear flow without Lorentz force, and the dash double-dotted line represents the shear flow with the upper Lorentz force. It is noteworthy that the asymmetry of the free stream causes a shift of the front stagnation point towards the high velocity side, thus increasing the pressure on the whole leeward and upper windward surface. Moreover, the field Lorentz force results in the pressure decreasing and the curves of $C_{p\mathrm{F}}^{\theta}$ moving downward.

The hydrodynamic force induced directly by wall Lorentz force is independent of flow field. Figure 6 displays the distributions of $C_{p\mathrm{W}}^{\theta}$, with the upper Lorentz force applied. All curves are of positive value and the pressure of upside is lower than that of underside distinctly while $C_{p\mathrm{W}}^{\theta}$ increases with Lorentz force increasing.

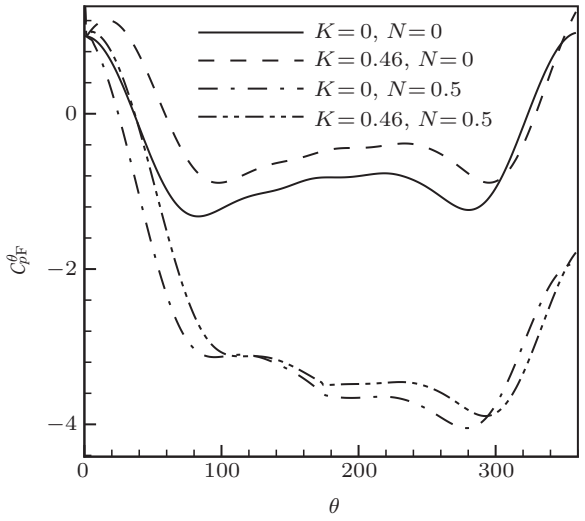


Fig. 5. Distributions of $C^{\theta}_{p\mathrm{F}}$ in shear flow with or without Lorentz forces.

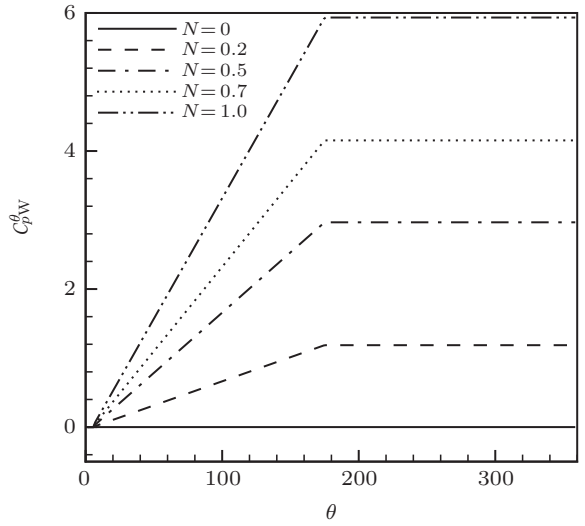


Fig. 6. Distributions of $C^{\theta}_{p\mathrm{W}}$ with the application of upper Lorentz force.

The distributions of $C^{\theta}_{d\mathrm{F}}$ at a given instant A are shown in Fig. 7. The shear flow causes a drag to increase on the upper windward surface and to decrease on the leeward surface. Contrariwise, the field Lorentz force causes a drag to decrease on the upper windward surface and to increase on the leeward surface. Usually, the total drag dominated by the drag on the leeward increases under the action of the upper field Lorentz force, if the Lorentz force is large enough.

The distributions of $C^{\theta}_{d\mathrm{W}}$ under the action of upper Lorentz force are shown in Fig. 8. $C^{\theta}_{d\mathrm{W}}$ is positive on the windward and it is negative on the leeward, and their absolute values also increase with Lorentz force increasing. In addition, $C_{d\mathrm{W}}$ dominated by $C^{\theta}_{d\mathrm{W}}$ of the leeward is always negative, which means that the wall Lorentz force always generates the thrust. Moreover, the thrust increases with Lorentz force increasing.

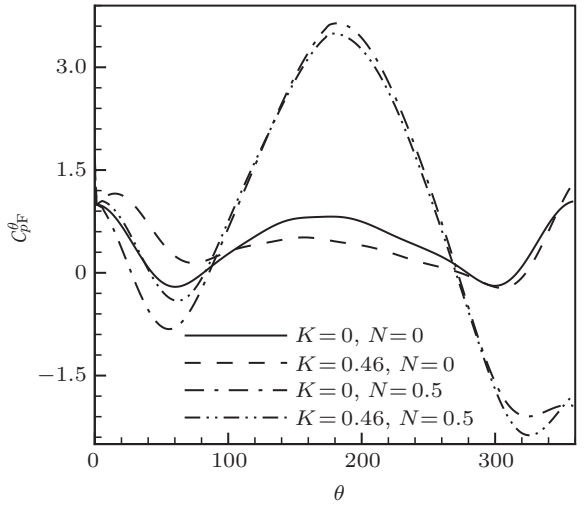


Fig. 7. Distributions of $C^{\theta}_{d\mathrm{F}}$ in shear flow, respectively, with and without Lorentz force.

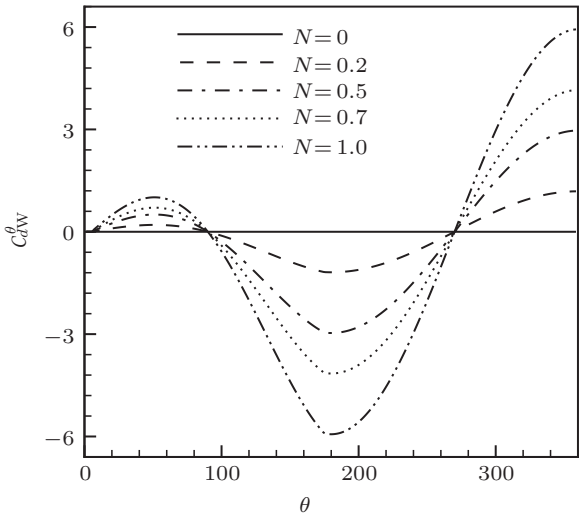


Fig. 8. Distributions of $C^{\theta}_{d\mathrm{W}}$ under the action of upper Lorentz force.

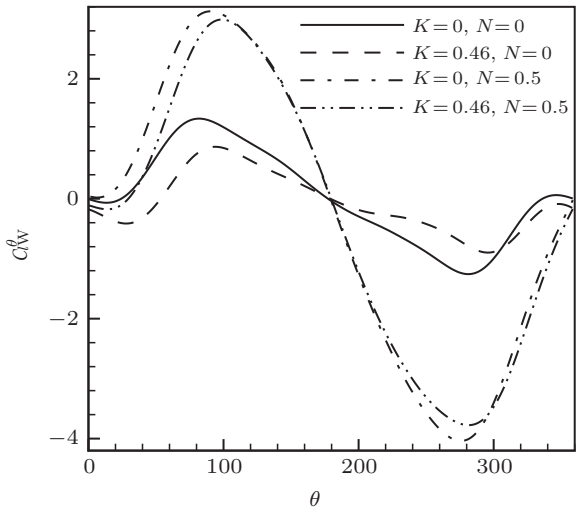


Fig. 9. Distributions of $C^{\theta}_{l\mathrm{F}}$ in shear flow, respectively, with and without Lorentz force.

The distributions of $C^{\theta}_{l\mathrm{F}}$ at a given instant A are shown in Fig. 9. The shear flow causes a lift to decrease on the upside

surface and to increase on the underside surface. Contrariwise, the field Lorentz force causes a lift to increase on the upside surface and to decrease on the underside surface. Usually, the total lift $C_{l\mathrm{F}}$ dominated by the lift on the underside surface directs toward the underside under the action of the upper field Lorentz force, as long as the Lorentz force is large enough.

The distributions of $C_{l\mathrm{W}}^{\theta}$ under the action of upper Lorentz force are shown in Fig. 10. $C_{l\mathrm{W}}^{\theta}$ is negative on the upper surface and it is positive on the lower surface, and their absolute values also increase with Lorentz force increasing. The total lift force $C_{l\mathrm{W}}$ dominated by $C_{l\mathrm{W}}^{\theta}$ on the lower surface is of positive value and increases with Lorentz force increasing, which means that the wall Lorentz force on the upper surface always raises the lift force.

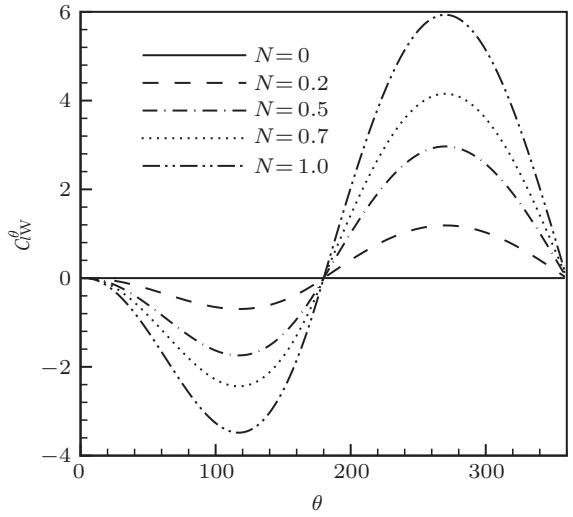


Fig. 10. Distributions of $C_{l\mathrm{W}}^{\theta}$ under the action of upper Lorentz force.

It is evident that the effects of the field Lorentz force on drag and lift are in contrast to those of the wall Lorentz force, and the wall Lorentz force dominates the drag and lift, which leads to the drag reduction and the lift increase. Phase diagrams of lift/drag with field and wall (upper) Lorentz force are shown in Fig. 11.

Compared with the diagram with $N = 0$ and $K = 0.46$, the phase diagram induced by field Lorentz force shrinks and moves downward and rightward, which means the lift reduction and the drag increase, whereas the phase diagram induced by wall Lorentz force moves upward and leftward with unchanged shape, leading to the drag reduction and the lift increase. However, the C_d–C_l diagram dominated by the wall Lorentz force moves upward and leftward.

The variations of the total lift/drag phase diagram with shear and upper Lorentz force are shown in Fig. 12. Compared with the case of $K = 0$ and $N = 0$, it is clear that the free stream shear, $K > 0$, causes the diagram to move downward and leftward and the upper Lorentz force induces the diagram to move upward and leftward. Therefore the lift force can be enhanced by upper Lorentz force with a moderate strength if the shear flow is encountered.

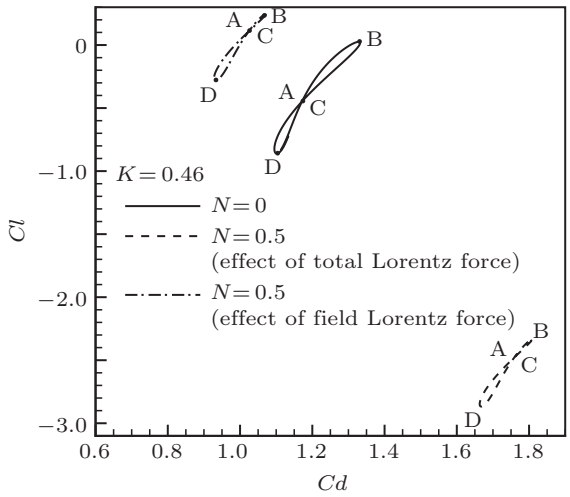


Fig. 11. Phase diagrams of lift/drag with field and wall (upper) Lorentz force.

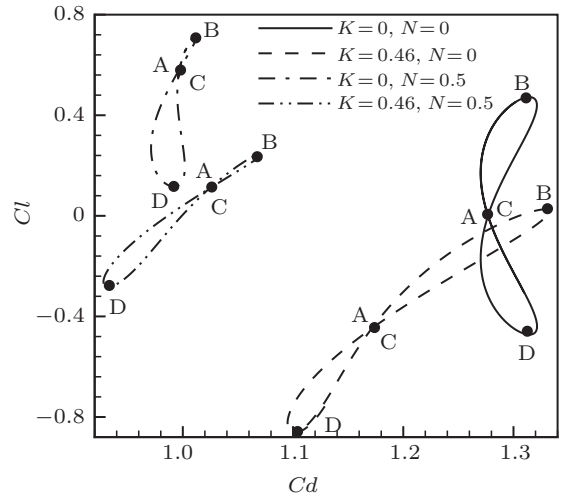


Fig. 12. Variations of total lift/drag phase diagram with shear and upper Lorentz force.

5. Experimental validations

The qualitative experiments are performed in a weak copper sulphate ($CuSO_4$) solution with almost the same density and conductivity as that of seawater. A long metal sheet is used as a support to mount the cylinder with a 2-cm diameter covered with the electrodes and magnets alternately. A strain gage sensor is installed at the top end of the sheet to measure the lift/drag force. Potassium permanganate ($KMnO_4$) is selected as a dark violet marker. In order to obtain a shear incoming flow, a hollow circular cylinder attached to a fixed beam is inserted into the tank which keeps still instead of rotating with the inner wall of the tank when the tank rotates. Thus the shear flow will be generated and become stable after approximately 10 min from startup according to the experiments. A detailed description about the experiments can be

found in Ref. [29].

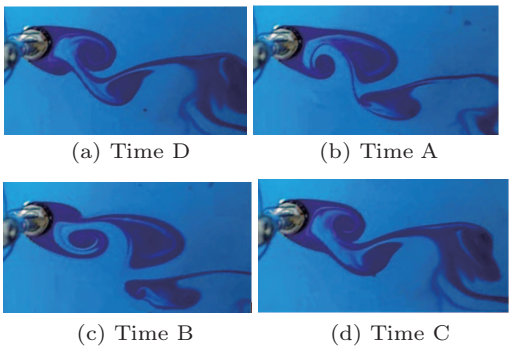


Fig. 13. (color online) Experimental visualizations of cylinder wake in shear flow at different instants.

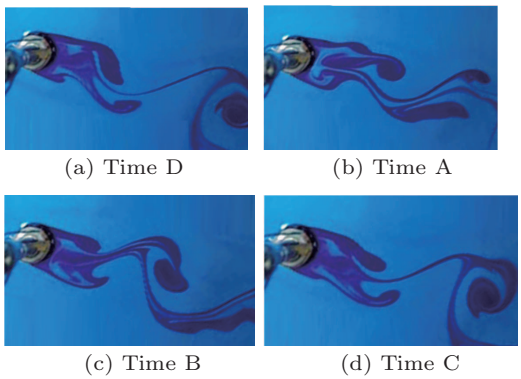


Fig. 14. (color online) Experimental visualizations of cylinder wake in shear flow with the action of upper Lorentz force.

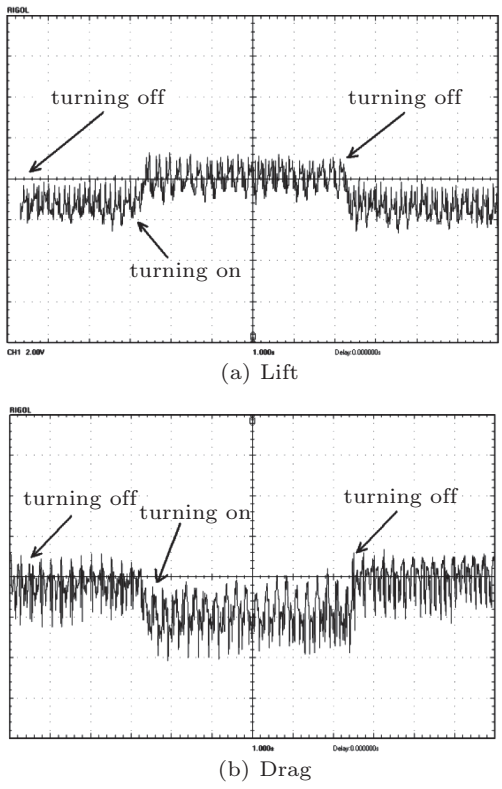


Fig. 15. Measured lift and drag in shear flow with upper Lorentz force.

Flow visualizations of cylinder wake in shear flow at different instants are shown in Fig. 13. As indicated in Fig. 13, the stagnation point shifts to the fast side of the free-steam due to the effect of shear flow, which causes the vortex street to be inclined toward the slow side of the free-stream.

The experimental visualizations of the cylinder wake controlled by upper Lorentz force with a moderate strength in a shear flow are shown in Fig. 14. The fluid momentum on the upper side increases with the application of Lorentz force, which leads to the increase of the vorticity, and the elongation of the shear layer connected with the upper surface of the cylinder.

Figures 15(a) and 15(b) show the measured lift and drag in shear flow under the action of upper Lorentz force, respectively. The lift increases and the drag decreases with the applied Lorentz force.

6. Conclusions

A numerical investigation is conducted by using the ADI algorithm and the FFT algorithm based on the governing equations in the exponential–polar coordinates. The distributions of hydrodynamic forces on the cylinder surface, i.e., wall pressure, drag, and lift induced by the Lorentz force are directly obtained from the corresponding equations derived in the paper.

For a uniform-shear flow ($K > 0$), the asymmetric diagram will move downward and leftward and the average lift force becomes negative (directed toward the downside). The Lorentz force generated by an electro–magnetic actuator can be classified into the field Lorentz force and the wall Lorentz force. Their effects on the lift and drag are contrary. For the Lorentz force exerted on the upper surface of the cylinder, the phase diagram moves downward and rightward by the field Lorentz force, thus resulting in the drag increase and the lift reduction, whereas it moves upward and leftward by the wall Lorentz force, leading to drag reduction and lift increase. Finally, the diagram is dominated by the wall Lorentz force, thus moving upward and leftward.

Therefore it is noteworthy that the upper Lorentz force, which enhances the lift force, can be used to overcome the lift loss due to the free-stream shear or the foil stall, the result for which is also obtained in the experiment.

References

[1] Roshko A 1955 *J. Aeronaut. Sci.* **22** 124
[2] Lee C B and Wu J Z 2008 *Appl. Mech. Rev.* **61** 030802
[3] Wu J Z, Lu X Y and Zhuang L X 2007 *J. Fluid Mech.* **576** 265
[4] Wu C J, Wang L and Wu J Z 2007 *J. Fluid Mech.* **574** 365
[5] Wang J J, Zhang P F, Lu S F and Wu K 2006 *Flow Turbulence and Combustion* **76** 83
[6] Li F, Yin X Y and Yin X Z 2009 *J. Fluid Mech.* **632** 199
[7] Mei D J, Fan B C, Huang L P and Dong G 2010 *Acta Phys. Sin.* **59** 6786 (in Chinese)

[8] Mei D J, Fan B C, Chen Y H and Ye J F 2010 *Acta Phys. Sin.* **59** 8335 (in Chinese)
[9] Jordon S K and Fromm J E 1972 *Physics of Fluids* **15** 972
[10] Tamura H, Kiya M and Arie M 1980 *Bull. JSME* **23** 1952
[11] Wu T and Chen C F 2000 *Acta Mechanica* **144** 71
[12] Lei C, Cheng L and Kavanagh K 2000 *Ocean Engineering* **27** 271
[13] Kang S 2006 *J. Fluid Structures* **22** 541
[14] Kiya M, Tamura H and Arie M 1980 *J. Fluid Mech.* **141** 721
[15] Kwon T S, Sung H J and Hyun J M 1992 *J. Fluids Eng. Trans. ASME* **114** 457
[16] Hayashi T, Yoshino F and Waka R 1993 *JSME Int. J. B* **36** 101
[17] Sumner D and Akosile O O 2003 *J. Fluid Structures* **18** 441
[18] Tang S and Aubry N 1997 *Physics of Fluids* **9** 2550
[19] Berger T, Kim J, Lee C and Lim J 2000 *Physics of Fluids* **12** 631
[20] Breuer K S, Park J and Henoch C 2004 *Physics of Fluids* **16** 897
[21] Mutschke G, Gerbeth G, Albrecht T and Grundmann R 2006 *Eur. J. Mech. B: Fluids* **25** 137
[22] Braun E M, Lu F K and Wilson D R 2009 *Progress in Aerospace Sciences* **45** 30
[23] Crawford C H and Karniadakis G E 1995 *AIAA*-952185
[24] Weier T, Gerbeth G, Mutschke G, Platacis E and Lielausis O 1998 *Experimental Thermal and Fluid Science* **16** 84
[25] Kim S and Lee C M 2001 *Fluid Dyn. Res.* **29** 47
[26] Posdziech O and Grundmann R 2001 *Eur. J. Mech. B: Fluids* **20** 255
[27] Chen Y H, Fan B C, Chen Z H and Zhou B M 2008 *Acta Phys. Sin.* **57** 648 (in Chinese)
[28] Zhang H, Fan B C and Chen Z H 2010 *Computers & Fluids* **39** 1261
[29] Zhang H, Fan B C, Chen Z H and Li Y L 2011 *Fluid Dyn. Res.* **43** 015506
[30] Chen Z H, Fan B C, Zhou B M and Li H Z 2007 *Chin. Phys.* **16** 1077
[31] Fey U, Konig M and Eckelmann H 1998 *Physics of Fluids* **10** 1547
[32] Mittal S and Kumar B 2003 *J. Fluid Mech.* **476** 303